Tailoring Optical and Dielectric Traits of SA Crystal Exploiting Glycine for Optoelectronics Applications

Syeda Bushra Tayyaba¹, M.D. Shirsat², S.S. Hussaini^{2*}

¹Crystal Growth Research Laboratory, Milliya Arts, Science and Management science College, Beed-431122, Maharashtra, India.

²RUSA Centre for Advanced Sensor Technology, Dr.Babasaheb Ambedkar Marathwada University, Aurangabad, 431001, Maharashtra, India.

Email: Shuakionline@yahoo.co.in

In current study, crystals of sulfamic acid (SA) and glycine-doped SA are being cultivated using the slow solvent evaporation technique to investigate glycine impact on linear-nonlinear optical, dielectric and microhardness traits of SA crystal. The crystallographic details of SA and glycine-doped (G-SA) have been determined via single crystal X-ray diffraction technique, catering structural insights. The qualitative analysis of glycine-doped SA has been done by using FTIR analysis. Optical transmittance enhancement in SA due to glycine is assessed from 200-1100 nm by means of UV-visible transmittance analysis. Glycine effect on second harmonic generation (SHG) efficiency and third-order nonlinear optical (TONLO) response are deduced through Kurtz-Perry powder test and Z-scan analysis. TONLO attributes have been comparatively examined exploring the close and open aperture Z-scan configurations and find the TONLO parameters of G-SA crystal. Comparative laser damage threshold analysis is performed using a 1064 nm Nd: YAG laser. The dielectric responses of SA and G-SA are evaluated within temperature range 30-90 °C. The Vickers microhardness analysis gauges the mechanical strength of SA and G-SA crystals.

Keywords: A Crystals, Optical properties, Nonlinear optics, Dielectric studies.

1. Introduction

Nonlinear optics is a globally acknowledged field that drives the advancement of cuttingedge technological applications reliant on nonlinear optical (NLO) crystals crafted from novel hybrid materials (organic/inorganic/semiorganic). Among the diverse array of material classes, inorganic crystals hold a particular allure due to their multifaceted structural,

physical, and mechanical attributes. Additionally, their possession of a modest nonlinear response garners significant attention in the realm of NLO device applications. Sulfamic acid (SA) emerges as an intriguing that crystallizes into an orthorhombic structure, boasting optical, mechanical, thermal and dielectric properties. These qualities have inspired our research group to embark on a reinvestigation of this crystal through the incorporation of additives. In recent years, the practice of doping additives into SA crystals has plaved a pivotal role in enhancing the inherent properties of SAcrystal[1-7]. The introduction of glycine into SA, in particular, emerges as a noteworthy additive capable of effectively tailoring the properties of SA [5–12]. Glycine, being the simplest amino acid with a zwitter ionic nature and pronounced charge polarization ability, as evidenced in the literature [1,13,14], holds the potential to exert a profound impact on the technologically significant traits of the SA crystal. Numerous researchers have delved into the effects amino acids. Notably, a group of researcher have documented the influence of L-Lysine hydrochloride on SA crystal [15]. Likewise, the impact of valine on optical, electrical, and mechanical characteristics in SA crystal has been elucidated by Fredseline et al. [16]. Similar to this effects of proline doping in SA is studied by Fredseline et al [16]. To the extent of our present knowledge, a notable void exists within the literature concerning a comprehensive exploration encompassing the linear and nonlinear optical, electrical, mechanical, and thermal characteristics displayed by glycine-doped SA crystals. It is discovered that there have been no findings regarding the improvement of SHG effectiveness following the doping of amino acids in SA crystals. Within the confines of this discourse, we introduce a thorough investigation, intricately dissecting the ramifications of glycine on the complete range of linear and nonlinear attributes intrinsic to SA crystals. Our research team has been the first to document the improved SHG performance of glycine-doped SA crystal. This undertaking serves to conspicuously underscore the substantial implications that arise, particularly in the context of distinct applications within nonlinear optics devices. In this study, our comprehensive investigation delved into the cultivation and analysis of sulfamic acid (SA) and glycine-doped SA crystals. Through meticulous techniques, we unraveled the profound impact of glycine on a spectrum of properties, spanning linear and nonlinear optics, dielectric responses, micro hardness, and etching behaviors. The X-ray diffraction and FTIR analysis provided a detailed understanding of structural arrangements and qualitative compositional traits. Notably, glycine's influence on optical enhancement, second harmonic generation and third-order nonlinear optical response was rigorously assessed. The laser damage threshold, temperature-dependent dielectric behavior and mechanical strength were also thoroughly examined. This collective exploration offers valuable insights into the potential applications and technological advancements of SA and glycine-doped SA crystals.

2. Materials and Methods

2.1 Methods of Experimental Analysis

Sulfamic acid (SA) was subjected to a dissolution process through HPLC, whereby it was gradually dissolved in two separate beakers, each containing 200 ml of deionized water. This method aimed to procure a saturated solution. In one of these beakers, a molar equivalent of glycine was introduced to the saturated SA solution. Subsequently, a stirring period of 4h

ensued, ensuring the thorough and uniform amalgamation of glycine within the SA solution. To promote the formation of crystals through gradual solvent evaporation and facilitate crystal nucleation, the beaker accommodating the saturated pristine SA solution, as well as the one with the glycine-doped SA solution, were placed within a controlled temperature environment. Over a span of 20 days, single crystals of both SA and glycine-doped SA (G-SA) were allowed to develop, as illustrated in Fig 1.

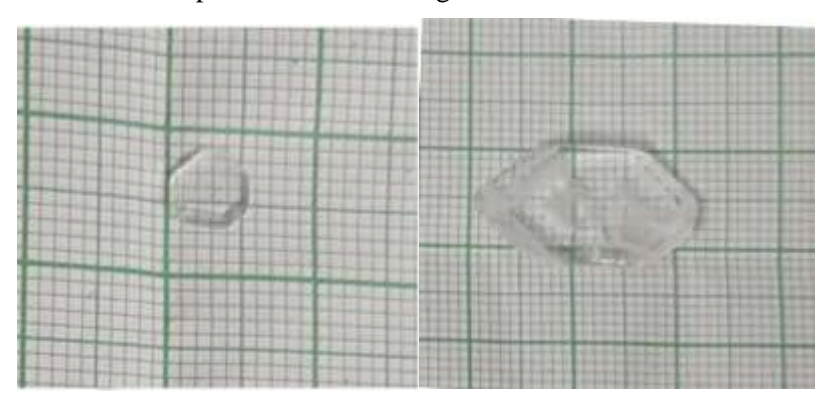


Fig 1(a) Crystal of SA

Fig1 (b) Crystal of G-SA

2.2 Methods of Characterization

The EnrafNonius CAD4 single crystal X-ray diffractometer was used to perform intricate X-ray diffraction analysis on an individual crystal specimen. Using a Bruker Alpha ATR spectrometer, the FTIR spectrum was meticulously recorded across a broad spectral range from 500 to 4000 cm⁻¹. The UV-visible spectrum, spanning from 200 to 1100 nm, was analysed using the SHIMADZU UV-1600 spectrophotometer. The determination of the second harmonic generation (SHG) response was orchestrated by harnessing the capabilities of a Q-switched Nd: YAG laser, which operated at a wavelength of 1064 nm, featuring meticulous parameters such as an 8 nm bandwidth, a repetition rate of 10 Hz, and a power output of 2.4 mW. Concurrently, the Z-scan analysis was executed by employing a continuous wave He-Ne laser operating at 632.8 nm. This was accompanied by the precise calibration of optical factors, encompassing a beam waist radius (ωa) measuring 1 mm, an optical path distance (Z) extending to 115 cm, a focal length of the converging lens (f) established at 20 cm, an aperture radius (ra) of 1 mm, and concentrated beam intensity (Io) of 3.8217 KW/cm². The quantification of the laser damage threshold energy was attained by enlisting a Nd:YAG laser crafted by Litron, emitting at a wavelength of 1064 nm. This procedure was conducted in conjunction with a converging lens endowed with a focal length (f) measuring 30 cm. The quantification of power was meticulously executed through the utilization of the EPM 200 energy/power meter. In the pursuit of dielectric analysis, varying temperatures of 30, 60, and 90 degrees Celsius were applied, and the instrument of choice was the HIOKI-3532 LCR meter, meticulously selected for this purpose. The determination of micro hardness properties was realized through the diligent application of the HMV-2T micro hardness tester. Furthermore, a detailed chemical etching analysis was undertaken, involving the meticulous capture of images at a magnification level of 40X, a task accomplished through the utilization of a microscope manufactured by the esteemed brand,

Micron.

3. Result and Discussion

3.1 XRD

Characterization of pure and G-SA crystals through single crystal X-ray diffraction analysis.

Thorough examination via XRD analysis has been meticulously executed to uncover the intricate crystallographic attributes inherent within both pure and G-SA crystals. The resulting XRD data has been meticulously compiled and organized elegantly presented within Table 1. Notably, this comprehensive data presentation unequivocally demonstrates the alignment of the scrutinized crystals with the orthorhombic crystal system. Furthermore, the insightful elucidation of the inherent space group for these crystals reveals a definitive assignment to the Pbca classification. A remarkable observation emerges from the comparison of unit cell parameters between the G-SA and SA crystals, unveiling subtle yet consequential alterations. This observation, in turn, serves as a compelling testament to the discernible influence exerted by glycine upon the crystalline lattice of SA.

Table 1: Comprehensive Data from Single Crystal X-ray Diffraction (XRD) Analysis

Crystal	Structure	Unit cell (Å)	Volume (Å) ³	Space group
SA	Orthorhombic	a = 8.073, b = 8.105, c = 9.25	605.243	Pbca
G-SA	Orthorhombic	a = 8.079, b = 8.110, c = 9.27	607.377	Pbca

3.2 FTIR Analysis:

Fig. 2 presents the transmittance FT-IR spectrum acquired from the cultured Glycine-doped S-A crystal. A meticulous scrutiny of the spectrum unveils prominent and distinct bands that correspond to specific modes of bonding. Particularly, the NH₃⁺ bonding mode becomes manifest with discernible peaks at frequencies of 3119 cm⁻¹ and 2881 cm⁻¹. Moreover, the presence of the OH stretching phenomenon is conspicuously evident, characterized by a distinctive band appearing at 2168 cm⁻¹. Noteworthy is the identification of the NH₃⁺ mode of vibration deformation, perceptibly captured by the distinctive band observed at 1532 cm⁻¹. Furthermore, vibrations attributed to the degenerated SO₃- stretching become discernible at 1230 cm⁻¹, while symmetric SO₃ stretching resonates at 1113 cm⁻¹. The astute observation of the rocking mode vibration NH₃⁺ at 954 cm⁻¹ substantially reinforces the genuine existence of zwitterions within the crystalline framework of the glycine SA compound. A salient addition is the identification of the N-S stretching vibration, eloquently captured at 660 cm⁻¹. Remarkably, all the observable infrared bands within the cultivated crystals seamlessly align with previously documented findings and exhibit a remarkable consistency with theoretically computed vibrational bands. This congruence unequivocally underscores the reliability and accuracy of the outcomes [17].

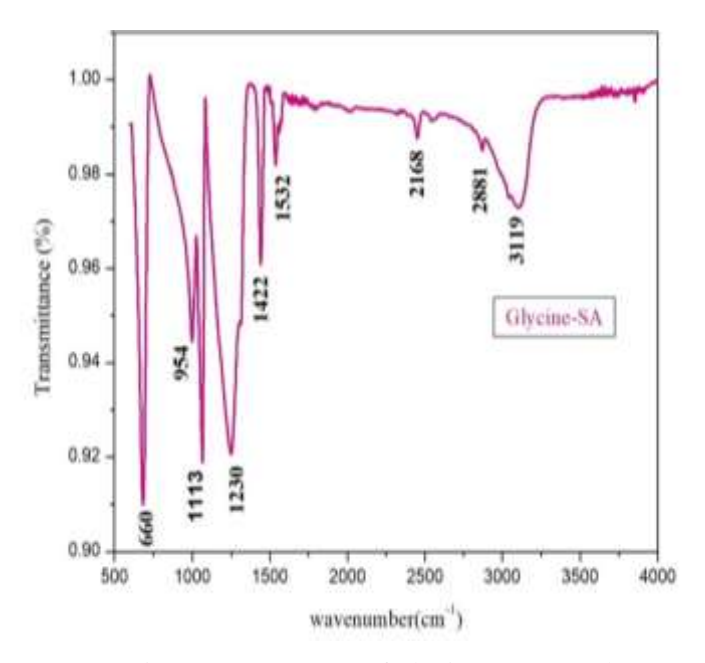


Fig 2. FTIR spectra of glycine SA crystal

3.3 UV visible Studies:

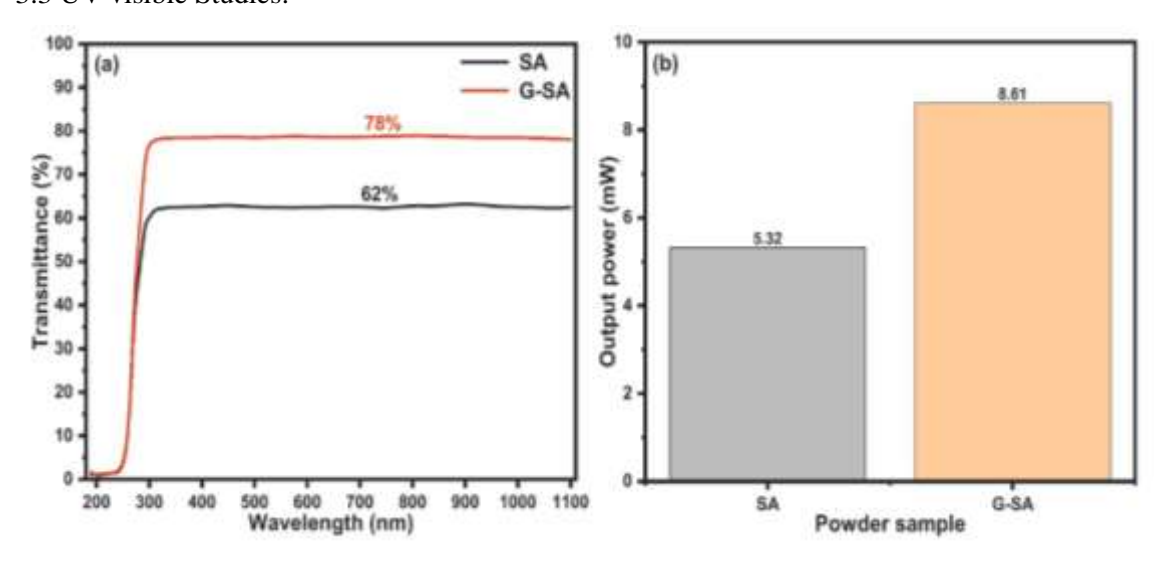


Fig. 3. (a) Transmittance spectrum (b) SHG response

The UV-visible spectrum, whether analyzed through transmittance or absorbance, emerges as a comprehensive manifestation of the intricate interplay between incident light and the optically active constituents, as well as the structural or crystalline imperfections inherent within the crystal lattice. This spectrum inherently acts as a blueprint, unravelling the intricate energy transitions intrinsic to the crystal and encapsulating the essence of its optical characteristics. Within this context, the transmittance spectrum of both SA and G-SA

crystals, offered by a thickness of 2 mm, has been assiduously documented and visually presented within Fig 3a. Evidently, this spectrum unveils an expanded window of transmission, characterized by a transmittance percentage of 62% for SA, which is notably elevated to 78% for the G-SA variant. The discernible manifestation of scattering or absorption of incident UV-visible light within the crystal matrix finds its origin in a confluence of internal factors, encompassing voids, defects, and grain boundaries, in tandem with external variables related to the crystal's geometric dimensions and orientation upon the crystal plane [18,19]. It is notable that the transmittance of the SA crystal undergoes a remarkable augmentation of 16% upon the introduction of glycine. This enhancement is attributed to inherent low absorption capacity of glycine, culminating in t

he amelioration of defect centers within the crystalline structure of G-SA. Such a substantial improvement assumes paramount significance, positioning the G-SA crystal as an exceedingly enticing candidate for non-linear optical (NLO) device applications [20].

3.4 SHG Analysis:

The emergence of second-order nonlinear optical (SONLO) activity in non-Centro symmetric solid materials intricately hinges upon the susceptibility (χ^2), an effect induced by the absorption of specific optical energy upon the irradiation of the sample. This SONLO response materializes as second harmonic generation (SHG) efficiency, a measurable attribute rigorously determined via the established Kurtz-Perry powder test [21]. In pursuit of this analysis, finely powdered samples of SA and G-SA were sieved and encapsulated within micro capillary tube of consistent bore, positioned within the optical path. Employing a Qswitched mode Nd:YAG laser in a multi-shot configuration directed at each respective sample, the resulting output power was quantified, as graphically represented in Fig. 3b. The empirical assessment culminated in an output power of 5.32 mW for SA and 8.61 mW for G-SA. Consequently, the SHG efficiency of the G-SA crystal outperformed that of SA by 1.61 times higher, a substantial enhancement attributed to inherent zwitterionic attributes introduced by the glycine dopant. This augmented SHG response is aptly juxtaposed against relevant literature benchmarks, elucidated within Table 2. Given its promising potential for second-order nonlinear optical activity, the G-SA crystal assumes a position of paramount significance within the realm of nonlinear optical (NLO) device applications.

Table 2: Comparative SHG efficiency analysis

Crystal	SHG signal
G-SA	8.61 mW
SA	5.32 mW

3.5 Z-Scan Analysis

The pioneering work of Bahae et al. introduced the Z-scan technique [22], an autonomous methodology uniquely tailored for the comprehensive assessment of third-order nonlinear optical (TONLO) traits. This encompasses fundamental attributes such as the absorption coefficient (β), refractive index (n^2), and cubic susceptibility ($\chi 3$) of the material. Through strategic integration of both close and open aperture schemes with a photodetector, the Z-scan configuration was meticulously established. This strategic arrangement yielded an intricate Z-scan transmittance (ZT) profile exclusively for the G-SA crystal. This distinctive

Nanotechnology Perceptions Vol. 20 No.6 (2024)

profile served as the cornerstone for the nuanced evaluation of the nature of n^2 and β characteristics, consequently furnishing invaluable insights into the intricate nonlinear optical attributes inherent to the G-SA crystal.

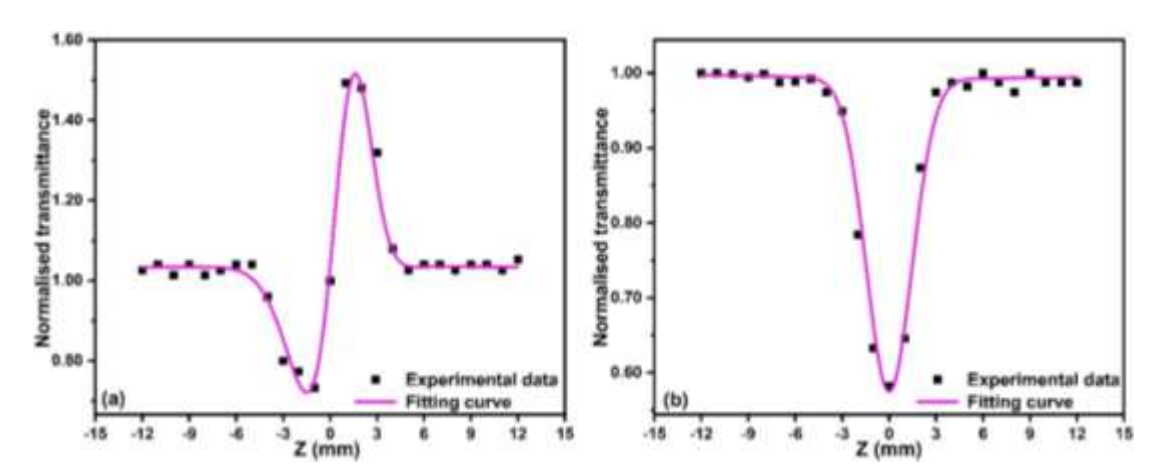


Fig. 4. ZT profile observed through (a) close and (b) open aperture

Fig. 4a and 4b illustrate the intricate dynamics of the close and open aperture Z-scan transmittance (ZT) profiles of the CS:G crystal. Notably, these profiles unveil a striking trend wherein the G-SA crystal manifests an augmentation in transmittance as the crystal is systematically translated from negative to positive positions relative to the focal point. This intriguing behavior inherently signals the positive nature of the nonlinear refractive index (n₂) intrinsic to the crystal's composition. The origin of this phenomenon resides in the irradiation of a high-frequency beam upon the crystal's surface, thereby inciting a remarkable anisotropic thermal lensing effect that attains prominence particularly at the nanoscale laser source regime. This affirmative n₂, duly facilitating a self-focusing (converging) influence, engenders a noteworthy Kerr lens mode-locking (KLM) phenomenon. The strategic exploitation of this effect bears substantial significance, especially in the realm of constructing laser stabilization mechanisms and fostering the generation of ultrafast pulses [1,22]. Moreover, the conspicuously intriguing open aperture ZT profile unveils a distinct pattern characterized by its minimal transmittance at the focal point, gradually yielding to a noteworthy increment as one progresses towards the peripheral regions. This remarkable

pattern mirrors the intricate characteristics synonymous with a reverse saturable absorption (RSA) profile. The manifestation of RSA aptly signifies a nonlinear absorption mechanism spurred by the interplay of multi-photon absorption (MPA) and excited state absorption (ESA) processes. The substantial RSA effect exhibited by the G-SA crystal effectively positions it as an enticing and auspicious contender for a range of applications spanning the optical limiting and biomedical domains [23,24]. The analysis of χ^3 aids to establish the interdependency of polarizing nature and high intermolecular charge transfer and its magnitude has been determined by evaluating several equations given in literature such as, $\Delta T_{p-v} = 0.406(1-S)^{0.25} |\Delta \phi|$, where $\Delta \Phi$ (phase shift), ΔT_{p-v} (peak-valley transmittance), S = [1-exp $(-2r_a^2/\omega_a^2)$] is linear aperture transmittance, r_a is aperture radius and ω_a is beam Nanotechnology Perceptions Vol. 20 No.6 (2024)

radius at aperture. The magnitude of n_2 is determined using formula, $n_2 = \frac{\Delta \phi}{KI_0L_{eff}}$, where K =

 2π / λ (λ is laser wavelength), I_0 is intensity of laser beam at focus (Z=0), L_{eff} = ([1-exp (αL)]/ α), is effective thickness of crystal sample which depends on linear absorption coefficient (α) and L thickness of sample. The β value of crystal has been calculated using

formula,
$$\beta = \frac{2\sqrt{2}\Delta T}{I_0 L_{eff}}$$
, where ΔT is one valley value at open aperture ZT. The χ^3 of G-SA

crystal was evaluated using, Re $\chi^{(3)}(esu) = 10^{-4} (\varepsilon_0 C^2 n_0^2 n_2) / \pi (cm^2 / W)$,

$$\operatorname{Im} \chi^{(3)}(esu) = 10^{-2} \left(\varepsilon_0 C^2 n_0^2 \lambda \beta \right) / 4\pi^2 (cm/W), \quad \chi^{(3)} = \sqrt{\left(\operatorname{Re} \chi^{(3)}\right)^2 + \left(\operatorname{Im} \chi^{(3)}\right)^2} , \text{ where }$$

 ε_0 is vacuum permittivity, n_0 is linear refractive index of sample and C is velocity of light in vacuum [22]. The impressive third-order nonlinear optical parameters exhibited by the SA and G-SA crystals are judiciously delineated within Table 3. These crystals, serving as beacons of promising TONLO attributes, proffer multifaceted potential across diverse domains, encompassing micro photolithography, holographic data storage, optical limiters, as well as photonic and optical sensor devices[25–27].

Table 3. TONLO parameter

Crystal	n ₂ (cm ² /W)	β (cm/W)	χ^3 (esu)	Reference
SA	4.09×10 ⁻⁹	3.81×10 ⁻⁸	8.74×10 ⁻⁹	[12]
G-SA	3.66×10 ⁻⁹	2.37×10 ⁻⁸	9.01×10 ⁻⁹	Present

3.6 Laser Damage Threshold

A profound understanding of the laser damage threshold (LDT) is pivotal for realizing the full potential of crystals in laser-driven photonics devices. The LDT is influenced by a myriad of factors, encompassing: (a) the presence of structural defects such as fractures, pits, cracks, scratches, and voids, (b) laser-specific parameters including pulse duration, fluence, and pulse rate, and (c) optical phenomena such as linear absorption, multiphoton absorption, stimulated Brillouin scattering, stimulated Raman scattering, and electron avalanche breakdown. In the context of the present investigation, both SA and G-SA crystals underwent exposure to a series of laser pulses, each spanning 10 seconds, thereby facilitating the observation of the crystals' damage thresholds. The initiation of surface damage is attributed to a synergistic interplay between thermally activated electron avalanches, photoionization of material, and multi-photon absorption processes. These intricate phenomena arise due to the localized irradiation of the laser beam, culminating in a cumulative effect. The ensuing damage materializes at the crystal's surface, materializing as fractures, cracks, melting, decomposition, and fusion [1]. The specific LDT values experienced by the SA and G-SA crystals have been meticulously documented and are comprehensively presented in Table 4. It is noteworthy that the tabulated data unequivocally demonstrates the susceptibility of the SA crystal to damage, occurring at an energy threshold of 85 mJ. In stark contrast, the G-SA crystal showcases a pronouncedly elevated resilience, enduring up to 110 mJ prior to the manifestation of damage. This profound disparity serves to underscore

a substantial enhancement in the laser damage threshold energy of the G-SA crystal—an impressive 129% increment when compared to its SA counterpart. Evidently, the strategic introduction of glycine as a dopant has emerged as a potent strategy for bolstering the laser damage threshold capabilities of the SA crystal, thereby augmenting its suitability for laser-driven applications.

Table 4. Laser damage threshold (LDT) data

Crystal	Shot Mode	Shot duration	Energy	Effect
SA	Multiple	10 seconds	45 mJ	No damage
		10 seconds	70mJ	No damage
		7 seconds	85 mJ	Damaged
G-SA	Multiple	10 seconds	40 mJ	No damage
		10 seconds	60 mJ	No damage
		10 second	90 mJ	No damage
		6 seconds	110mJ	Damaged

3.7 Dielectric Studies

The dielectric investigation serves as a methodological avenue for elucidating the potential utility of crystals across a diverse spectrum of technological domains, encompassing but not confined to the realms of electro-optics, photonics, and optoelectronics. In the present scholarly inquiry, a meticulous exploration of the dielectric response has been meticulously undertaken, spanning a thermal range spanning from 30 to 90 °C, with a probing frequency of 100 kilohertz. The intricate dielectric attributes, notably the dielectric constant (expressed as $\varepsilon_r = Cd/\varepsilon_0 A$, wherein C symbolizes capacitance, d signifies the thickness of the specimen, A denotes the area of the sample, and ε0 stands as the permittivity of free space), and the dielectric loss (designated as $\delta = \tan^{-1}(\varepsilon_{r}/\varepsilon_{0})$), have been graphically represented for both the SA and G-SA crystals in Fig. 5a and 5b, respectively. The manifestation of ε_r finds explication in distinct polarization mechanisms, embracing electronic, ionic, dipolar, and space charge polarization (SCP), each evincing an acute susceptibility to variations in frequency and temperature. Scrutinizing Fig 5a, a conspicuous elevation in the ε_r values of both SA and G-SA crystals is discernible with an ascent in temperature. This phenomenon can be ascribed to the waning responsiveness of the polarization mechanism at lower thermal regimes, while at elevated temperatures, the amplification in ε_r primarily derives impetus from the ascendancy of SCP, a supposition corroborated by antecedent investigations [28,29]. Notably, the ε_r attributed to the G-SA crystal exhibits a discernibly inferior magnitude compared to its SA crystal counterpart, thereby underscoring the discernible influence exerted by glycine upon the dielectric constant of the SA crystal. The inquiry casts a spotlight upon crystals endowed with attributes such as porosity, defects, micro-macro fissures, and stochastic surface undulations, concomitant with the presence of grain boundaries, which conspicuously manifest in the δ values [28–31]. Fig. 5b elucidates a strikingly congruent graphical correspondence between the δ values and the dielectric constant of the cultivated crystals. Although both the SA and G-SA crystals evince an escalated δ with mounting temperature, the δ value associated with the G-SA crystal remains appreciably subjugated in relation to its SA crystal analogue. This divergence serves as an

indicative compass directing attention to the pivotal role assumed by glycine in the amelioration of electrically active defects within the G-SA crystal, thereby engendering a diminished δ value. Consequently, the G-SA crystal, with its concurrent lower ϵ_r and δ attributes, emerges as a preeminent contender vis-à-vis the SA crystal. In summation, the exhaustive dielectric scrutiny not only illuminates the intricate choreography of polarization mechanisms along with their concomitant thermal sensibilities but also accentuates the propitious attributes intrinsic to the G-SA crystal, characterized by diminished dielectric loss and augmented dielectric constant. This comparison substantiates the G-SA crystal's propitious standing as a front-runner for envisaged application within the ambit of optoelectronic devices.

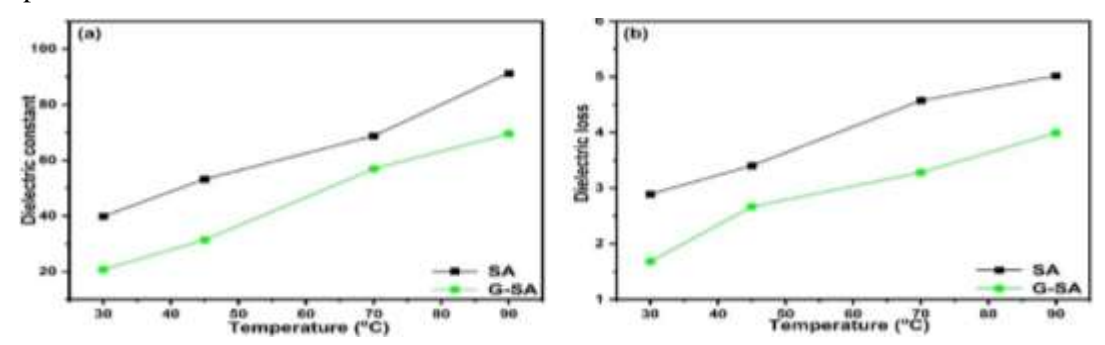


Fig. 5.Temperature dependent response of (a) dielectric constant (b) dielectric loss

3.8 Micro hardness studies

A comparative Vicker's microhardness analysis has been employed within 25-100 gm to investigate variation in hardness number ($H_v = 1.8544 \ P/d^2 \ Kg/mm^2$, where P is applied load ingm, d is diagonal length in mm), Mayer's index (n) and elastic stiffness coefficient (C_{11}) of SA and G-SA crystal.

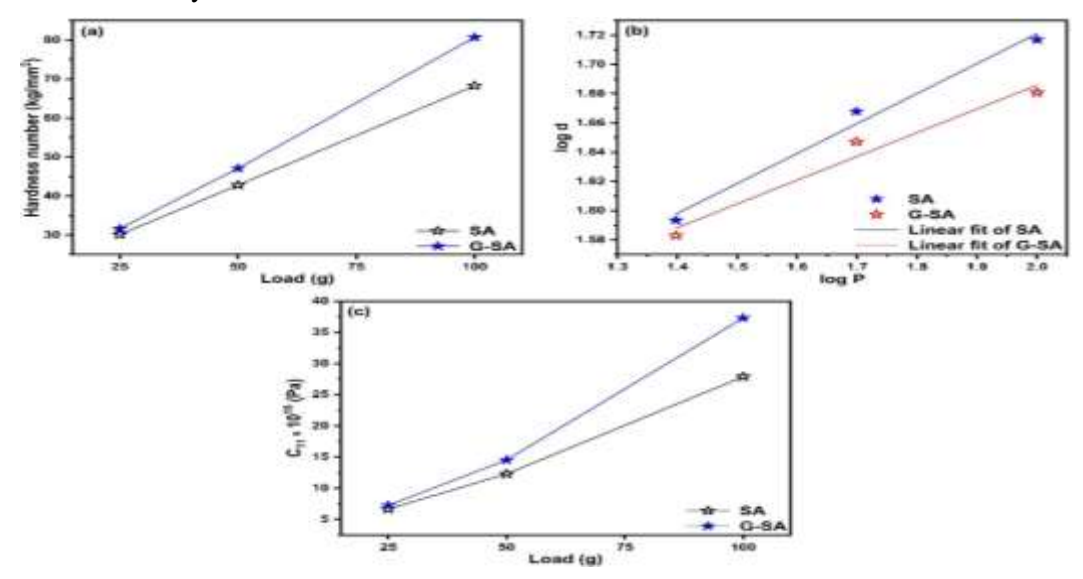


Fig. 6. (a) Load vsH_v (b) log P vs log d (c) Load vs C₁₁

Nanotechnology Perceptions Vol. 20 No.6 (2024)

The hardness variations (Hv = $1.8544 \text{ P/d}^2 \text{ Kg/mm}^2$, with P denoting the applied load in gm and d representing diagonal length in mm) are visually presented in Fig 6a. The graphical depiction unveils a proportional increase in the hardness value (Hv) for both the SA and G-SA crystals, corresponding to the escalating applied indented load, thus validating the emergence of the reverse indentation size effect (RISE) [32]. Importantly, the Hv of the G-SA crystal markedly surpasses that of the SA crystal, signifying that the G-SA crystal demands a greater stress magnitude to induce deformation in contrast to the SA crystal. Material classification into the categories of hardness or softness is unveiled through the determination of the Meyer's index (n), derived from the slope of the logarithmic plot of applied load (log P) against the logarithm of diagonal length (log d), depicted in Figure 6b. Research by Onitsch substantiated that a material falls under the domain of (i) softness if n > 2, and (ii) hardness if n < 2 [33]. The observed n value surpasses 2, thereby confirming the soft nature of both the SA and G-SA crystals. The trajectory of the elastic stiffness coefficient (C₁₁) is showcased in Figure 6c, enabling an assessment of the intermolecular bond strength amidst neighbouring atoms [34]. Evidently, an increament in the applied load is associated with a proportional enhancement in the magnitude of C_{11} . Additionally, it is noteworthy that the value of C₁₁ attributed to the SA crystal markedly exceeds that of the G-SA crystal. Given the remarkable hardness attributes inherent in the G-SA crystal, it assumes a pivotal role in the design of mechanically resilient devices.

4. Conclusion

A single crystal of glycine was formed after being doped in SA and it underwent several characterizations. Single crystal X-ray diffraction (XRD) determined unit cell dimensions, confirming orthorhombic crystal structure and Pbca space group for SA and G-SA crystals. FTIR analysis validated functional groups in SA and glycine-doped SA. UV-visible spectral analysis (200-1100 nm) showed glycine increased SA transmittance by 16%. Enhanced second SHG of G-SA was 1.61 times SA. Z-scan analysis confirmed promising two-photon nonlinear optical (TONLO) response of G-SA, modifying SA's negative nonlinear refractive index (n2) and absorption to positive n2 and reverse saturable absorption. G-SA exhibited higher laser damage threshold (110 mJ) than SA (85 mJ). Dielectric studies revealed glycine significantly reduced SA's dielectric constant and loss, beneficial for optoelectronic devices. Vickers micro hardness analysis indicated glycine enhanced SA's mechanical strength.

References

- 1. M.I. Baig, M. Anis, M.D. Shirsat, H.H. Somaily, S.S. Hussaini, Exploring linear-nonlinear optical, dielectric and microscopic traits of sulphamic acid crystal exploiting Zn2+ for photonic device applications, J. Mater. Sci. Mater. Electron. 32 (2021) 16445–16455.
- 2. S.K. Jat, N. Vijayan, A. Krishna, J. Philip, S. Verma, I. Bdikin, B. Singh, G. Bhagavannarayana, S.K. Halder, Nucleation kinetics, growth, mechanical, thermal and optical characterization of sulphamic acid single crystal, CrystEngComm. 15 (2013) 10034–10042.
- 3. M.S. Pandian, U.C. In, P. Ramasamy, P. Manyum, M. Lenin, N. Balamurugan, Unidirectional growth of sulphamic acid single crystal and its quality analysis using etching, microhardness, HRXRD, UV–visible and Thermogravimetric-Differential thermal characterizations, J. Cryst.

- Growth. 312 (2010) 397-401.
- 4. M. Lenin, N. Balamurugan, P. Ramasamy, Growth and characterization of sulphamic acid single crystals grown by Sanakaranarayanan-Ramasamy (SR) method, Cryst. Res. Technol. J. Exp. Ind. Crystallogr. 42 (2007) 39–43.
- 5. D. Jaishree, G. Kanchana, R. Kesavasamy, Investigations on growth, optical and thermal properties of sulphamic acid single crystals, Adv. Condens. Matter Phys. 2014 (2014).
- 6. F.A. Kanda, A.J. King, The crystal structure of sulfamic acid1, J. Am. Chem. Soc. 73 (1951) 2315–2319.
- 7. I.M. Pritula, O.N. Bezkrovnaya, A. V Lopin, M.I. Kolybaeva, V.M. Puzikov, R.I. Zubatyuk, O. V Shishkin, V.Y. Gayvoronsky, Optical properties of KDP crystals doped with pyrenetetrasulfonic acid salt, J. Phys. Chem. Solids. 74 (2013) 452–456.
- 8. K. Bouchouit, Z. Sofiani, B. Derkowska, S. Abed, N. Benali-Cherif, M. Bakasse, B. Sahraoui, Investigation of crystal structure and nonlinear optical properties of 2-methoxyanilinium nitrate, Opt. Commun. 278 (2007) 180–186.
- 9. S.P. Ramteke, M. Anis, M.I. Baig, M. Shkir, V. Ganesh, G.G. Muley, Eye-catching modification in external morphology, photoluminescence and SHG efficiency of NH4H2PO4 crystal: A consequence of influential presence of tartaric acid, Optik (Stuttg). 158 (2018) 634–638.
- 10. Y. Li, M. Wang, T. Zhu, X. Meng, C. Zhong, X. Chen, J. Qin, Synthesis, crystal structure and properties of a new candidate for nonlinear optical material in the IR region: Hg 2 BrI 3, Dalt. Trans. 41 (2012) 763–766.
- 11. Y.-H. He, Y.-Z. Lan, C.-H. Zhan, Y.-L. Feng, H. Su, A stable second-order NLO and luminescent Cd (II) complex based on 6-hydroxynicotinic acid, Inorganica Chim. Acta. 362 (2009) 1952–1956.
- 12. C. Chen, G. Liu, Recent advances in nonlinear optical and electro-optical materials, Annu. Rev. Mater. Sci. 16 (1986) 203–243.
- 13. S.S. Hussaini, N.R. Dhumane, V.G. Dongre, P. Ghughare, M.D. Shirsat, Growth and characterization of glycine doped KDP single crystal for optoelectronics applications, Optoelectron. Adv. Mater. Rapid Commun. 1 (2007) 707–711.
- 14. N.R. Dhumane, S.S. Hussaini, V.G. Dongre, M.D. Shirsat, Influence of glycine on the nonlinear optical (NLO) properties of zinc (tris) thiourea sulfate (ZTS) single crystal, Opt. Mater. (Amst). 31 (2008) 328–332.
- 15. J. Arumugam, M. Selvapandiyan, S. Chandran, M. Srinivasan, P. Ramasamy, Crystal growth, optical, thermal, mechanical and third-order nonlinear optical properties of L-lysine hydrochloride-doped sulphamic acid single crystals for optical applications, Appl. Phys. A. 126 (2020) 1–11.
- 16. F.R.S. VITHEL, R. MANIMEKALAI, STRUCTURAL AND OPTICAL ANALYSIS OF GLYCINE SUBSTITUTED SULPHAMIC ACID, Stoch. Model. (n.d.).
- 17. Y. Yang, S. Pan, X. Hou, C. Wang, K.R. Poeppelmeier, Z. Chen, H. Wu, Z. Zhou, A congruently melting and deep UV nonlinear optical material: Li 3 Cs 2 B 5 O 10, J. Mater. Chem. 21 (2011) 2890–2894.
- 18. M.S. Pandian, N. Pattanaboonmee, P. Ramasamy, P. Manyum, Studies on conventional and Sankaranarayanan–Ramasamy (SR) method grown ferroelectric glycine phosphite (GPI) single crystals, J. Cryst. Growth. 314 (2011) 207–212.
- 19. M. Anis, S.P. Ramteke, M.D. Shirsat, G.G. Muley, M.I. Baig, Novel report on γ-glycine crystal yielding high second harmonic generation efficiency, Opt. Mater. (Amst). 72 (2017) 590–595.
- C.R. Raja, A.A. Joseph, Crystal growth and comparative studies of XRD, spectral studies on new NLO crystals: 1-Valine and 1-valinium succinate, Spectrochim. Acta Part A Mol. Biomol. Spectrosc. 74 (2009) 825–828.
- 21. S.K. Kurtz, T.T. Perry, A powder technique for the evaluation of nonlinear optical materials, J.

- Appl. Phys. 39 (1968) 3798-3813.
- 22. M. Sheik-Bahae, A.A. Said, T.-H. Wei, D.J. Hagan, E.W. Van Stryland, Sensitive measurement of optical nonlinearities using a single beam, IEEE J. Quantum Electron. 26 (1990) 760–769.
- 23. Y.-D. Zhang, Z.-Y. Zhao, C.-B. Yao, L. Yang, J. Li, P. Yuan, The nonlinear absorption and optical limiting in phenoxy-phthalocyanines liquid in nano-and femto-second regime: experimental studies, Opt. Laser Technol. 58 (2014) 207–214.
- 24. M. Anis, M.I. Baig, G.G. Muley, S. AlFaify, M.A. Khan, Impact of increasing concentration of l-alanine environment on structural, UV–vis, SHG efficiency, luminescence and dielectric traits of zinc thiourea chloride (ZTC) crystal, Optik (Stuttg). 185 (2019) 317–324.
- 25. N. Vijayan, G. Bhagavannarayana, S.K. Halder, S. Verma, J. Philip, R. Philip, B. Rathi, X-ray topography, photopyroelectric and two-photon absorption studies on solution grown benzimidazole single crystal, Appl. Phys. A. 110 (2013) 55–58.
- 26. Y.-T. Fan, D.-X. Xue, G. Li, H.-W. Hou, C.-X. Du, H.-J. Lu, Synthesis, crystal structures, and third-order nonlinear optical properties of two novel complexes of H4edbbp with Zn (II), Cd (II), J. Mol. Struct. 707 (2004) 153–160.
- 27. M.D. Zidan, M.M. Al-Ktaifani, A. Allahham, Nonlinear optical investigation of the Tris (2', 2-bipyridyl) iron (II) tetrafluoroborate using z-scan technique, Opt. Laser Technol. 90 (2017) 174–178.
- 28. M. Anis, G.G. Muley, M.I. Baig, G. Rabbani, H.A. Ghramh, S.P. Ramteke, Doping effect of Ni2+ on structural, UV-visible, SHG efficiency, dielectric and microhardness traits of KH2PO4 (KDP) crystal, Optik (Stuttg). 178 (2019) 752–757.
- 29. B.D. Hatton, K. Landskron, W.J. Hunks, M.R. Bennett, D. Shukaris, D.D. Perovic, G.A. Ozin, Materials chemistry for low-k materials, Mater. Today. 9 (2006) 22–31.
- 30. M. Saravanakumar, J. Chandrasekaran, M. Krishnakumar, B. Babu, G. Vinitha, M. Anis, Experimental and quantum chemical studies on SHG, Z-scan and optical limiting investigation of 2-amino-5-bromopyridinium trifluoroacetate single crystal for optoelectronic applications, J. Phys. Chem. Solids. 136 (2020) 109133.
- 31. S. Rajyalakshmi, K.R. Rao, B. Brahmaji, K. Samatha, T.K.V. Rao, G. Bhagavannarayana, Optical investigations on Tb3+ doped l-Histidine hydrochloride mono hydrate single crystals grown by low temperature solution techniques, Opt. Mater. (Amst). 54 (2016) 74–83.
- 32. N. Bhuvaneswari, K. Baskar, R. Dhanasekaran, Growth and characterization of tris thiourea magnesium zinc sulphate single crystals, Optik (Stuttg). 126 (2015) 3731–3736.
- 33. M. Anis, G.G. Muley, M.D. Shirsat, S.S. Hussaini, Single crystal growth, structural, optical, mechanical, dielectric and thermal studies of formic acid doped potassium dihydrogen phosphate crystal for NLO applications, Cryst. Res. Technol. 50 (2015) 372–378.
- 34. T. Pal, T. Kar, Studies on mechanical properties of an organic nonlinear optical crystal, Mater. Sci. Eng. A. 437 (2006) 235–239.